Chapter 2

Earthquake Centroid Locations Using Calibration from Ambient Seismic Noise

This chapter has been published as:

Zhan, Z., Wei, S., Ni, S., and Helmberger, D. (2011), Earthquake centroid locations using calibration from ambient seismic noise, Bulletin of the Seismological Society of America, Volume 101, Number 3, Pages 1438-1445.

2.1 Abstract

Earthquakes occur in complex geology, making it difficult to determine their source parameters and locations because of uncertainty in path effects. We can avoid some of these problems by applying the cut-and-paste (CAP) method, which allows for timing shifts between phases, assuming a 1D model, and determines source parameters. If the travel times or lags of the phases due to path effects are known relative to a reference model, we can locate the events' centroid with surface waves without knowledge of the 3D velocity structure. Here, we use ambient seismic noise for such a calibration. We cross correlate the seismic stations near the earthquake with stations 100–300 km away to obtain the 10–100-s surface wave Green's functions. The new method is tested in Southern California to locate the 2008 Chino Hills earthquake, which proves

consistent with the epicenter location from P waves. It appears possible to use the location offset between the high-frequency P-wave onset relative to the centroid to provide a fast estimate of directivity.

2.2 Introduction

The characterization of earthquakes in near real time is one of the major themes in the seismic monitoring community. Another is addressing events with sparse data that commonly occur in remote areas or historical events that occurred before dense instrumentation. All of these issues can benefit from using more of the regional records beyond the initial P waves. The objective of this report is to explore the use of surface waves to aid in source estimation, which requires crustal velocity models. Several new methods have been developed to retrieve such structures based on the cross correlation of ambient seismic noise (station-to-station) and conventional (source-to-station) inversions (Tape et al., 2010). The latter approach provides the most broadband results, containing both body-wave phases and surface waves. Generally, the travel times of P waves are used to locate events because the arrivals display little dispersion, and velocity models can be calibrated in timing by artificial sources with known location and origin time. Surface waves are more difficult to calibrate in that they involve earthquakes. In this case, one must separate the source excitation from the propagation or path effects.

The first approach, station-to-station, does not have this problem because we generally know where the stations are located, and ambient seismic noise (ASN) can be used to calibrate the timing of the surface waves (Shapiro et al., 2005; Ma et al., 2008). Thus, we propose locating earthquakes with the help of surface waves where the trade-offs issue just mentioned has been eliminated. Because locating earthquakes in near real time is the most useful, we will apply the cut-and-paste (CAP) method

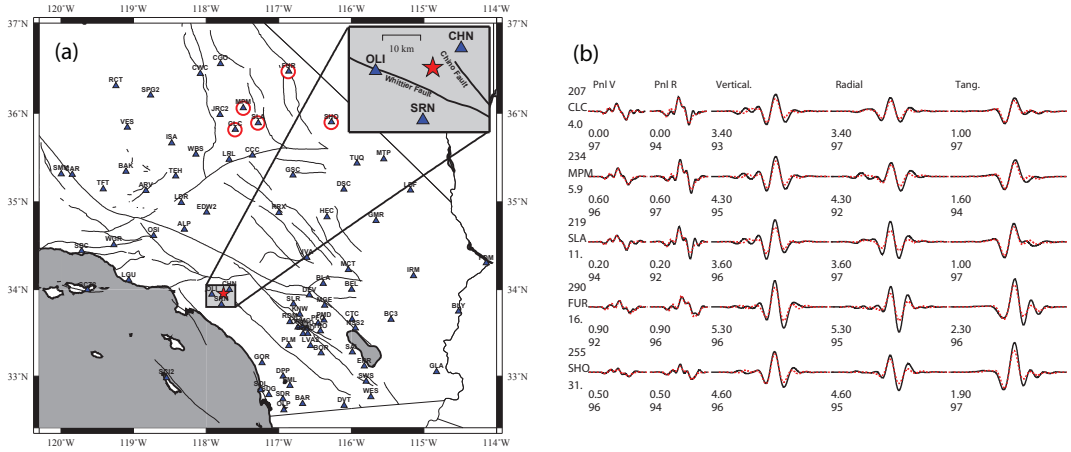

Figure 2.1: (a) Locations of the 29, July 2008 Chino Hills earthquake (star) and stations (triangles) used in this study, along with (b) a sample of CAP inversions. The five stations used in this sample CAP inversion are highlighted by circles in (a). In (b), the station names are expressed in three letters with their distances in kilometers above the letters. The numbers below the letters state the azimuth in degrees. Results in matching *Pnl* and surface waves are given on the right with data in solid lines and fits in dashed lines. The numbers below the segments state the timing shifts and the cross correlations. Positive time shifts indicate that the synthetic needs to be shifted back or that the data arrives late. Note that the Rayleigh wave is 4.6 s late, while the Love wave is 1.9 s for station SHO.

to estimate the depth and mechanism. This method fits the Rayleigh and Love wave segments by allowing travel-time shifts relative to a reference model. If these shifts can be determined by previous events, the surface waves can be used in combination with body waves to locate events with sparse networks (Zhu et al., 2006; Tan et al., 2006). Here, we will use ASN for the surface-wave calibration, and the well-calibrated TriNet array for testing, see Figure 2.1. In particular, we will readdress the well-studied Chino Hills event (Hauksson et al., 2008). In short, we will use ASN to calibrate paths connecting the Chino Hills event with the TriNet array as a proof-of-concept test.

2.3 Data Processing and Analysis

This earthquake was widely felt and reported by Hauksson et al. (2008). The CAP technique has been used to estimate the focal mechanism and depth (Zhu and Helmberger, 1996). The method fits the Rayleigh and Love wave segments by allowing travel-time shifts relative to a 1D reference model with some example waveform fits given in Figure 2.1b. The delays of the surface waves displayed here can be predicted from prior events to within a second (Tan et al., 2010) if they have high cross correlations (cc>0.85). A small number of stations can then be used to produce a relatively good mechanism and location using complete records, as demonstrated in Tan et al. (2006). Thus, the Program for Array Seismic Studies of the Continental Lithosphere (PASSCAL) deployments can be used to calibrate permanent stations and maintain accuracy (Tan et al., 2006). In short, the key information is how well we can predict these path corrections with ASN. The 5–100-s period surface waves are well recorded by the TriNet array. To calibrate the travel times of these surface waves, the three closest stations (CHN, OLI, and SRN) were chosen as the virtual sources in noise cross correlation (Figure 2.1).

These three stations are cross correlated with the TriNet stations with epicentral distances from 100 km to 350 km, which recorded clear 5–100-s period surface waves. The 5–100-s surface wave empirical Green's functions have been regularly retrieved using ambient seismic noise cross correlation across the United States (Bensen et al., 2008). Our cross-correlation procedure is similar to that given by Bensen et al. (2007) and Lin et al. (2008). Twelve months of continuous long-period records (LHE, LHN, LHZ) in 2006 are downloaded from Southern California Earthquake Center's (SCEC) Seismogram Transfer Program (STP) and cut into daily segments. After removal of mean, trend, and instrumental response, the seismograms are bandpass filtered between 5 s and 100 s. To remove the effect of earthquakes, we first filter the

original seismograms between 15 s and 50 s to emphasize the surface waves of earthquakes, and then calculate their envelope functions. The inverse of these smoothed envelope functions are used to weight the corresponding seismograms between 5 s and 100 s trace by trace. This procedure has been proven to be effective in suppressing earthquake signals (Bensen et al., 2007). Cross correlations between all three components (east, north, and vertical, ENZ-ENZ) are then computed over daily intervals and stacked. To separate the Rayleigh and Love waves, the ENZ-ENZ noise cross-correlation functions (NCFs) are rotated to give the radial-transverse-vertical (RTZ-RTZ) components (Lin et al., 2008). We also test rotating seismograms to RTZ components before cross correlation and find that the NCFs look almost identical. The positive and negative sides of the rotated NCFs are folded and summed to give the final NCFs. The resulting vertical-vertical (Z-Z) and transverse-transverse (T-T) NCFs are used for Rayleigh and Love waves, respectively.

The 10–100-s passband proved the most useful, so we will begin with an example of Rayleigh wave and Love wave comparison, Figure 2.2a. As the focal mechanism and depth affect phases of surface waves, it is not appropriate to compare earthquake surface waves and NCFs directly. Instead, the time differences are measured by cross correlating the earthquake records or the NCFs (Figure 2.2a, solid lines) with 1D synthetics (Figure 2.2a, dashed lines) in time windows of 60 s around the predicted surface wave travel times. We use the SCEC epicenter location of the earthquake and focal mechanism and depth from Hauksson et al. (2008) to calculate the 1D synthetics, assuming the standard SoCal model (Dreger and Helmberger, 1993). For NCFs, a vertical/tangential point force is placed at the virtual sources on the free surface to calculate the Rayleigh/Love wave synthetics. The numbers above and below the seismograms are the time shifts in seconds and cross-correlation coefficients. Figure 2.2b is a schematic to show the meaning and relations of these time shifts. The true centroid location of the earthquake is the star A, initial estimation of the location

(SCEC epicenter in this example) is A', and the seismograms are recorded at station C (SHO in this example). The time shifts from the earthquake are attributed to two factors: (1) error in epicentral distance AC-A'C due to location error and (2) the velocity anomaly between the earthquake A and station C. To obtain a better centroid location, we need to calibrate the path effect. Station B (CHN in this example) is close to the earthquake, and the NCFs between B and C are the empirical Green's functions between B and C with B as a virtual source. Because BC is close to AC, the NCFs will sample a similar velocity anomaly as AC; hence, this provides a calibration of the path effect.

The results for the full network are presented in Figure 2.8 for Rayleigh waves and Figure 2.9 for Love waves (both figures are available in supplementary material). The corresponding (5–10 s) results are given in Figures 2.10 and Figure 2.11. To be useful in locating, these figures require a high degree of fit, maximum cross correlation between data/NCF and synthetic cc>0.8. We summarize these fits in a bar diagram, Figure 2.12. The percentages of NCFs with cc>0.8 at 10–100 s is 88% for both Rayleigh and Love waves, whereas they drop to 47% and 36% in the 5–10-s band. Apparently, the surface geology is too complex at these shorter wavelengths to obtain accurate delays. A more complete comparison of matching the earthquake data is presented in Figure 2.13.

A particularly convenient way to view the delays and cc's is in the form of spider diagrams as presented in Figure 2.3 and Figure 2.4. The overall high similarity among the spider diagrams of the three virtual sources, especially for the stations with high cross-correlation coefficients, indicates that the NCFs with the three different virtual sources are sampling similar velocity structures and hence provide a stable calibration of the path effect. The similarity between earthquake and noise spider diagrams indicates that the SCEC epicenter is quite close to the true centroid location and that the time shifts for the earthquake are dominated by the path effects. The adjustment

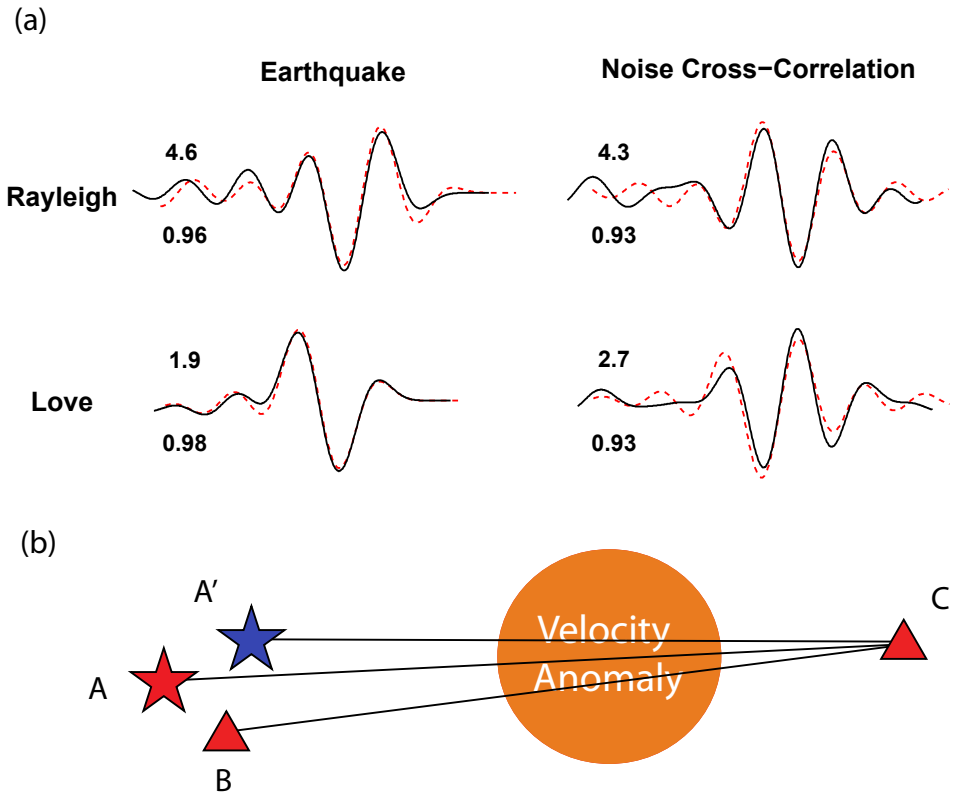

Figure 2.2: Illustration of locating an earthquake with noise cross correlation as path calibration. (a) Observed travel time differences with respect to the 1D SoCal model for both Rayleigh waves (upper row) and Love waves (lower row) of the Chino Hills earthquake recorded at SHO (left column) and the noise cross-correlation functions (NCFs) between CHN and SHO (right column). Dash lines are the synthetic seismograms from 1D SoCal model. The numbers above and below the seismograms are the time shifts in seconds and cross-correlation coefficients. The durations of all the seismograms are 60 s. (b) The earthquake location is given by the star A with an estimate at the star A'. Station B (CHN in this example) is close to the earthquake, and the NCFs between B and C are the empirical Green's functions between B and C with B as a virtual source. Because BC is close to AC, the NCFs will sample the same velocity anomaly as AC, hence providing a calibration of the path effect.

of the centroid location with respect to the SCEC epicenter will be based on the small differences between earthquake and noise spider diagrams.

Before relocating the earthquake, we test the true accuracy of the method by locating a virtual source station, SRN, as displayed in Figure 2.5. When locating with the 1D SoCal model, time shifts from SRN (Figure 2.5, open squares in the left column, upper and lower rows for Rayleigh and Love waves, respectively) will be entirely attributed to the error of the source location used in calculating the 1D synthetics, i.e., the true location of SRN. An iterative least-square algorithm is used to solve the inverse problem. The result converges quickly after one or two iterations. The residual time shifts are shown as open circles in the left column of Figure 2.5. The resulting location is shown in Figure 2.6 with a 95% confidence limit, offset approximately 6 km to the south-southeast (SSE) of the true location. If the calibration from OLI is used, a large part of the time shifts due to path effect is removed, as shown in the right column of Figure 2.5 as open squares. The greatly reduced variance of the time shifts indicates that the location used in calculating 1D synthetics (true SRN location) is a good estimation. This is confirmed by the resulting location shown in Figure 2.6, which is only approximately 1 km to the southeast of the true location. Replacement of the L2 norm in the inverse algorithm with an L1 norm, which is less sensitive to outlier measurements (e.g., Shearer, 1997), does not make any obvious difference in this example. A similar analysis for the other stations is given in Figures 2.14 and Figure 2.15 and is summarized in Figure 2.6 with all the results. The 1D model locations are systematically offset to the south by about 6 km due to overall slower velocity structure to the north relative to the 1D SoCal model. The large 95% confidence limits of 1D locations are caused by the complicated velocity heterogeneities. After the noise calibration, the path effect is largely removed, and the resulting locations are much closer to the true locations with much smaller 95% confidence limits.

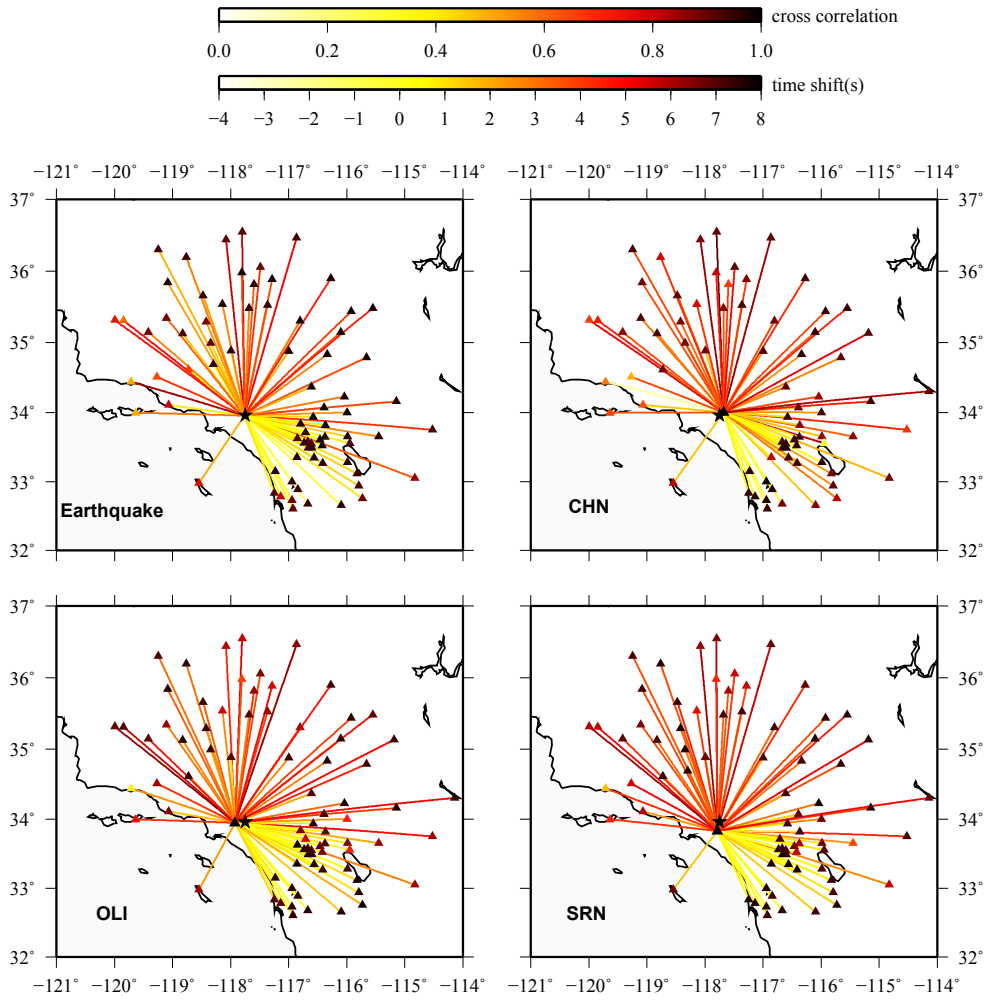

Figure 2.3: Spider diagrams of the Rayleigh wave time shifts with respect to the 1D SoCal model for the Chino Hills earthquake (star in the center) and three closest stations CHN, OLI, and SRN (triangles) as virtual sources. The colors of the paths indicate the time shifts, and the station colors indicate the cross-correlation coefficients.

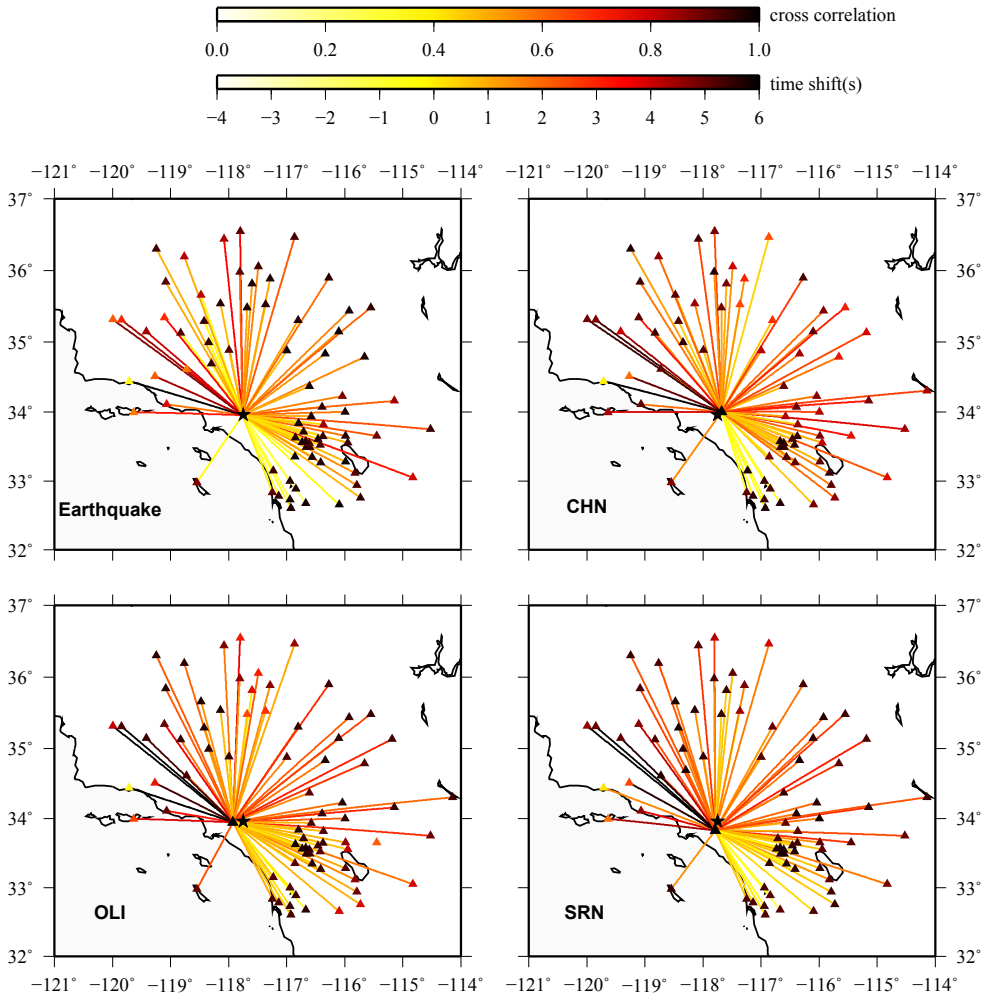

Figure 2.4: Similar to Figure 2.3, but for Love waves.

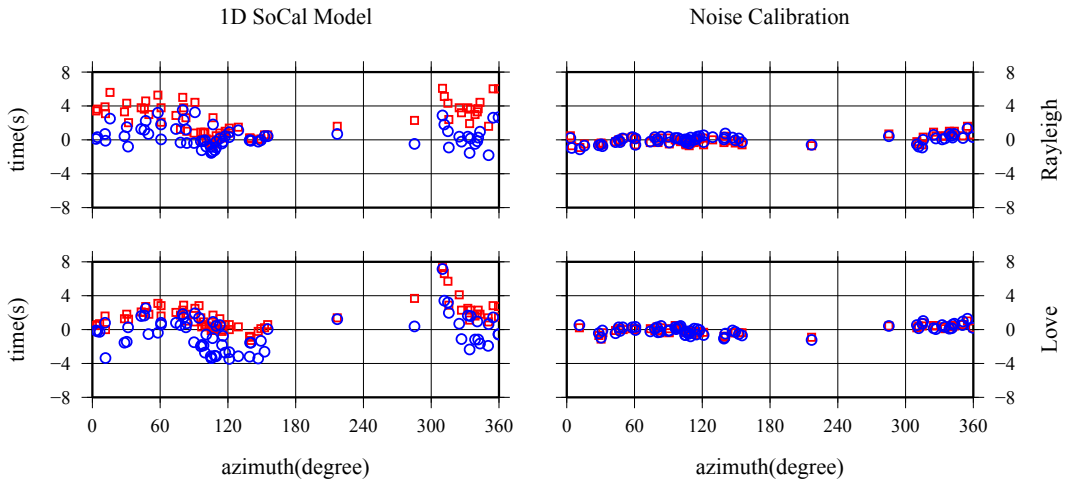

Figure 2.5: Location of virtual source station SRN based on the 1D SoCal model (left) compared to using station corrections (calibration) from OLI (right). The squares refer to the delays (timing offsets) measured from the cross correlations of NCFs taken from Figure 2.3 and Figure 2.4 with the 1D Green's functions, Rayleigh (top) with Love (bottom). The circles are residual time shifts after least-square relocation. The plots on the right use corrections obtained from station OLI. The resulting locations for virtual source SRN are shown in Figure 2.6.

The two large stars in Figure 2.6 are the epicenters of the earthquake from the SCEC catalog and the earthquake given by Hauksson et al. (2008), labeled EH. Small stars with ellipses are the relocated earthquake centroid locations with the 1D model or noise calibrations and their 95% confidence limits. Similar to the 1D locations of virtual sources, the 1D location of the earthquake is also largely offset to the south and has a large confidence limit. After the noise calibrations from three virtual sources (CHN, OLI, and SRN) as displayed in Figure 2.7, the resulting centroid locations are offset 1–3 km to the west of the estimated epicenters, which appear to be well resolved. Thus, the difference between the epicenter location and centroid location suggests rupture towards the west. This type of analysis is expected to show larger source location differences with larger magnitudes and can be used to provide quick estimates of directivity. The two arrows perpendicular to the Whittier fault and the Chino fault show the fault dips, although these dips are not well known (Hauksson

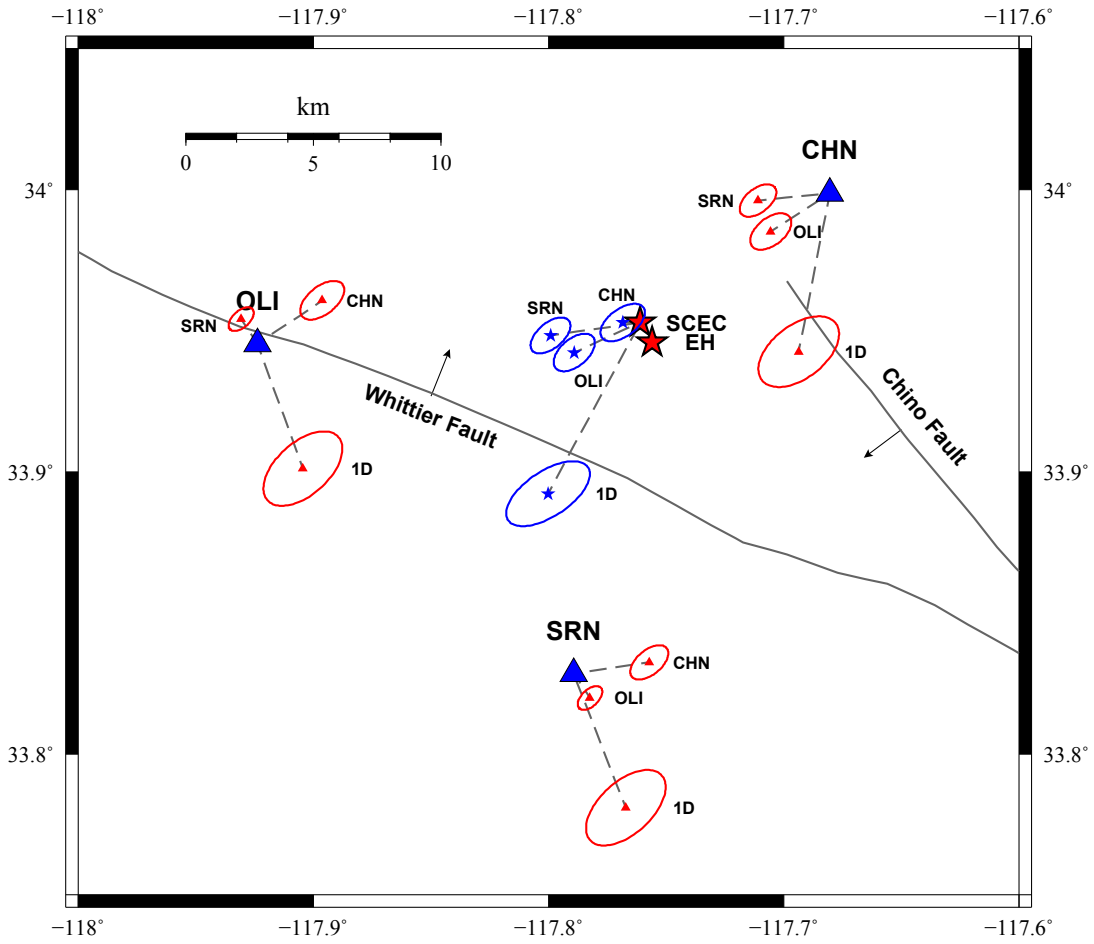

Figure 2.6: Estimated locations of the virtual sources and the earthquake with 1D SoCal model or noise calibrations. Large triangles are the true locations of the three virtual source stations CHN, OLI, and SRN. The dashed lines connecting small triangles with ellipses are the relocated virtual sources with their 95% confidence limits. Two large stars, labeled as SCEC and EH, are epicenter locations from the SCEC catalog and Egill Hauksson's catalog (Hauksson et al., 2008). The dashed lines connecting small stars with ellipses are the relocated earthquake centroid locations with their 95% confidence limits, using the 1D model, or noise calibrations from CHN, OLI, and SRN, respectively.

et al., 2008).

2.4 Discussion and Conclusions

Passive imaging with earthquake coda waves and ambient seismic noise has been primarily used to study structure, but more recently has been used for many other applications. A common use is to measure dispersion between two points as done with earthquake data (Campillo and Paul, 2003), or this technique can be used in combination with the earthquake surface wave technique (Lin et al., 2008). Here, we are interested in shorter paths where surface waves are less dispersive and dominated by the Airy phase. Its overall period is controlled by the surface layering and its timing by the S velocity in the source layer (Song et al., 1996). Thus, they become useful for locating events at local and near-regional distances. However, they have disadvantages relative to the P wave in that they are at longer periods and are influenced by the radiation pattern. Because P waves can be observed at high frequencies, they are easy to measure and also easily calibrated from explosion data. Numerous calibration explosions have been conducted globally for this purpose, and thus, this is a well-developed method for refining source locations.

In contrast, local surface waves must be addressed in terms of mechanism and location together because small changes in mechanism can change delay times (Wei et al., 2012), and thereby influence location. However, the NCFs have well-known source terms and locations and, therefore, are independent of P-wave calibration and provide unique information about travel times.

Because the source mechanism and surface wave delays are closely related, it becomes particularly advantageous to use this information together by coupling the CAP method and the location as discussed in the previous paragraph. However, it does require a local 1D model or regional model that is compatible with observed

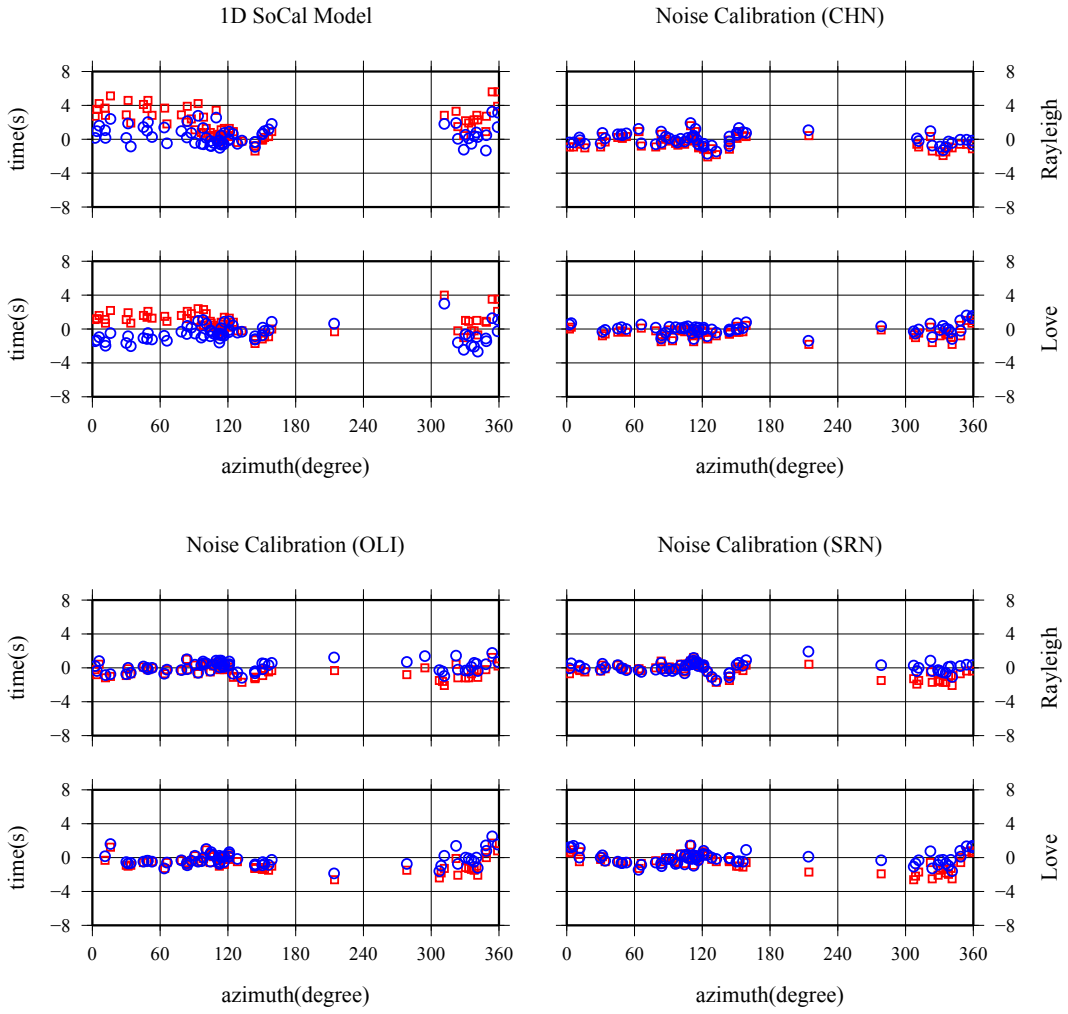

Figure 2.7: This figure is similar to Figure 2.5, but locates the Chino Hills earthquake with the 1D SoCal model or noise calibration from three virtual sources CHN, OLI, and SRN. In the upper left panel, squares refer to time delays measured by cross correlating earthquake records with synthetic seismograms from the 1D SoCal model (earthquake cases in Figure 2.3 and Figure 2.4). Circles are the residual time delays after least-square relocation of the earthquake centroid. The other three panels are similar, except that travel-time calibrations from the three virtual sources, CHN, OLI, and SRN are used, respectively, in each of the three panels. The resulting centroid locations with confidence limits are displayed in Figure 2.6 (small stars with ellipses).

airy phases. Fortunately, at 10 s, this restriction is not great in that simple models consisting of a soft surface layer, 2–4 km, and a uniform crust prove effective (e.g., Tan et al. (2010) for Southern California, Zhu et al. (2006) for Tibet, and Ni and Helmberger (2010) for Korea).

In summary, we have introduced a new method for locating earthquakes by extending the CAP methodology using path calibrations from ambient seismic noise. Because the CAP method proves effective in determining mechanisms without a detailed crustal structure, it is particularly useful in combination with NCFs in studying local seismicity from PASSCAL experiments and USArray. Such applications will be addressed in future efforts.

Acknowledgments

Continuous seismic record and earthquake seismograms used in this study were obtained from the IRIS Data Management Center or Southern California Earthquake Center. Some plots were made using the Generic Mapping Tools version 4.2.0. Two anonymous reviewers and the editor provided helpful comments to improve the article. This work was supported by USGS NEHRP grant G10AP00048, NSFC 40821160549, CAS KZCX2-YW-116-1, and CEA program 200808078, 200708035.

References

Bensen, G. D., Ritzwoller, M. H., Barmin, M. P., Levshin, A. L., Lin, F., Moschetti, M. P., Shapiro, N. M., and Yang, Y. (2007). Processing seismic ambient noise data to obtain reliable broad-band surface wave dispersion measurements, Geophys. J. Int. 169, 1239-1260.

Bensen, G. D., Ritzwoller, M. H., and Shapiro, N. M. (2008). Broad-band ambient

noise surface wave tomography across the United States, J. Geophys. Res. 113, B05306.

Campillo, M., and Paul, A. (2003). Long range correlations in the seismic coda, Science 299, 547-549.

Dreger, D. S., and Helmberger, D. V. (1993). Determination of source parameters at regional distances with three-component sparse network data, J. Geophys. Res. 98, no. B5, 8107-8125.

Hauksson, E., Felzer, K., Given, D., Giveon, M., Hough, S., Hutton, K., Kanamori, H., Sevilgen, V., Wei, S., and Yong, A. (2008). Preliminary report on the 29 July 2008 Mw 5.4 Chino Hills, eastern Los Angeles basin, California, earthquake sequence, Seismol. Res. Lett. 79, 838-849.

Lin, F. C., Moschetti, M. P., and Ritzwoller, M. H. (2008). Surface wave tomography of the western United States from ambient seismic noise: Rayleigh and Love wave phase velocity maps, Geophys. J. Int. 173, 281-298.

Ma, S., Prieto, G. A., and Beroza, G. C. (2008). Testing community velocity models for southern California using the ambient seismic field, Bull. Seismol. Soc. Am. 98, 2694-2714.

Ni, S., Helmberger, D. V., and Pitarka, A. (2010). Rapid source estimation from global calibrated paths, Seismol. Res. Lett., 81, no. 3, 498-504.

Shapiro, N. M., Campillo, M., Stehly, L., and Ritzwoller, M. H. (2005). High-resolution surface-wave tomography from ambient seismic noise, Science 307, 1615-1618.

Shearer, P. M. (1997). Improving local earthquake locations using the L1 norm and

waveform cross correlation: Application to the Whittier Narrows, California, aftershock sequence, J. Geophys. Res. 102, B4, 8269-8283.

Song, X. J., Helmberger, D. V., and Zhao, L. (1996). Broadband modeling of regional seismograms: The Basin and Range crustal structure, Geophys. J. Int. 125, 15-29.

Tan, Y., Song, A., Wei, S., and Helmberger, D. V. (2010). Surface wave path corrections and source inversions in southern California, Bull. Seismol. Soc. Am. 100, no. 6, 2891-2904.

Tan, Y., Zhu, L., Helmberger, D. V., and Saikia, C. (2006). Locating and modeling regional earthquakes with two stations, J. Geophys. Res. 111, B1, 1306-1320.

Tape, C., Liu, Q., Maggi, A., and Tromp, J. (2010). Seismic tomography of the southern California crust based on spectral-element and adjoint methods, Geophys. J. Int. 180, 433-462.

Wei, S., Z. Zhan, Y. Tan, S. Ni, and D. Helmberger (2012), Locating earthquakes with surface waves and centroid moment tensor estimation, J. Geophys. Res., 117, B04309.

Zhu, L., Tan, Y., Helmberger, D. V., and Saikia, C. (2006). Calibration of the Tibetan Plateau using regional seismic waveforms, Pure Appl. Geophys. doi: 10.1007/s00024-006-0073-7, 1193-1213.

Supplementary figures: Cross-correlation, waveform comparisons, and source locations with 1D model and noise calibration

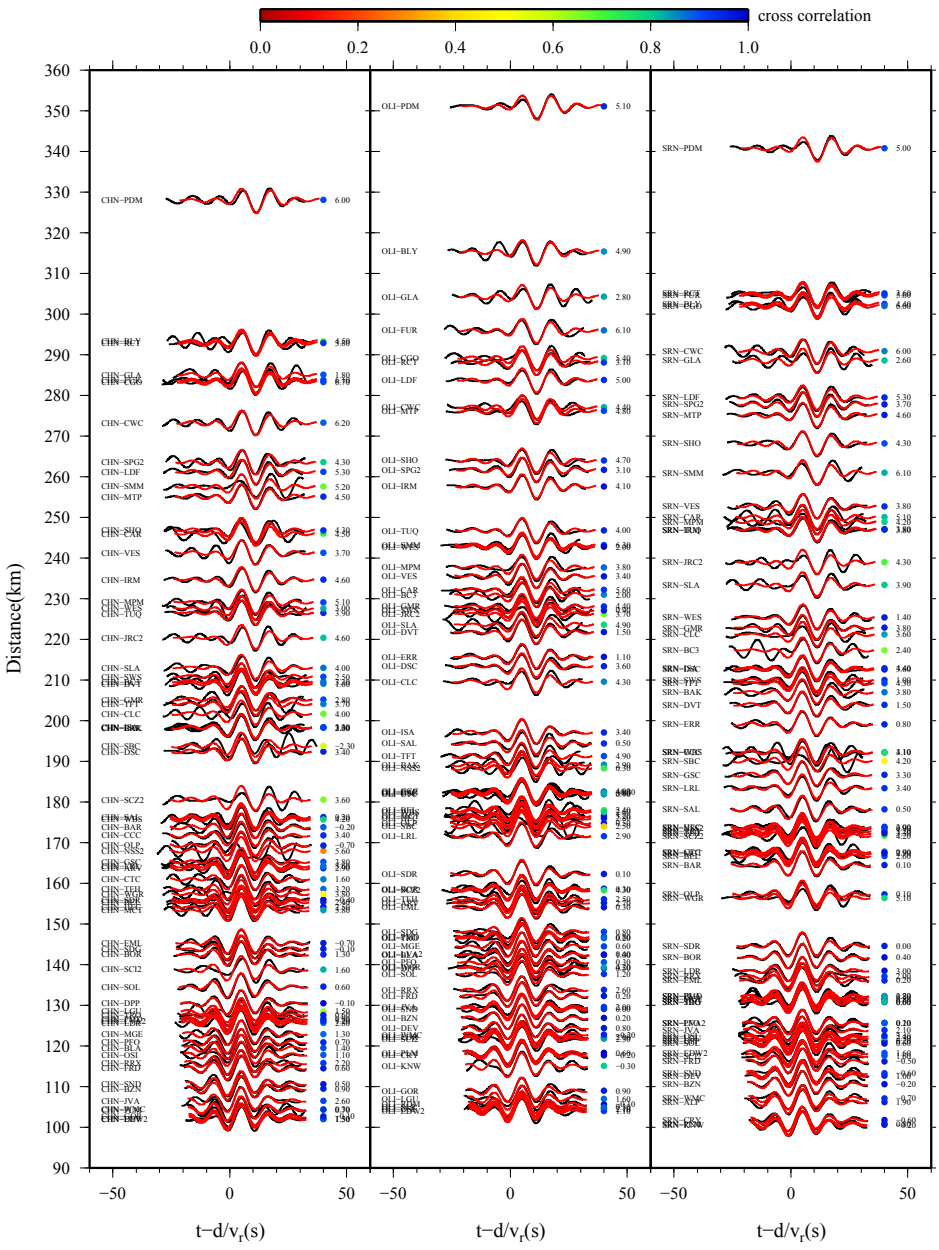

Figure 2.8: Measurement of time shifts between 10-100s Z-Z NCFs (Rayleigh waves, black lines) and 1D synthetic seismograms (red lines) by cross-correlation. The station pairs are classified by their source stations (CHN, OLI or SRN) and displayed in three columns. The names of stations for each NCF are shown to the left of the seismograms. The maximum cross-correlation coefficient (colored dot) and the corresponding time shift are shown on the right. A reduction velocity of Vr=3.44km/s is used that best aligns the synthetics.

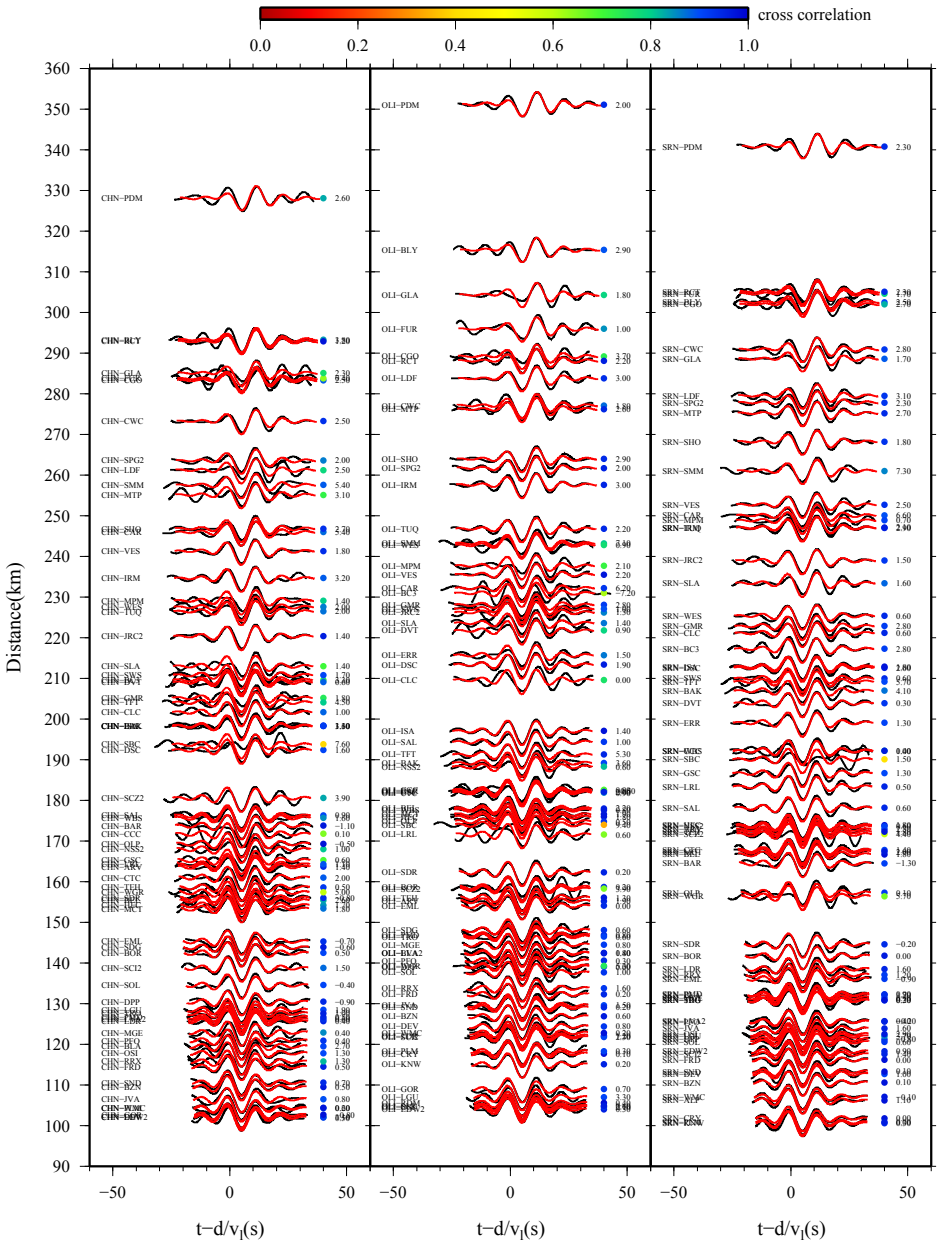

Figure 2.9: The same as Figure 2.8, but for 10-100s T-T NCFs (Love waves). A reduction velocity of Vl=3.73km/s is used.

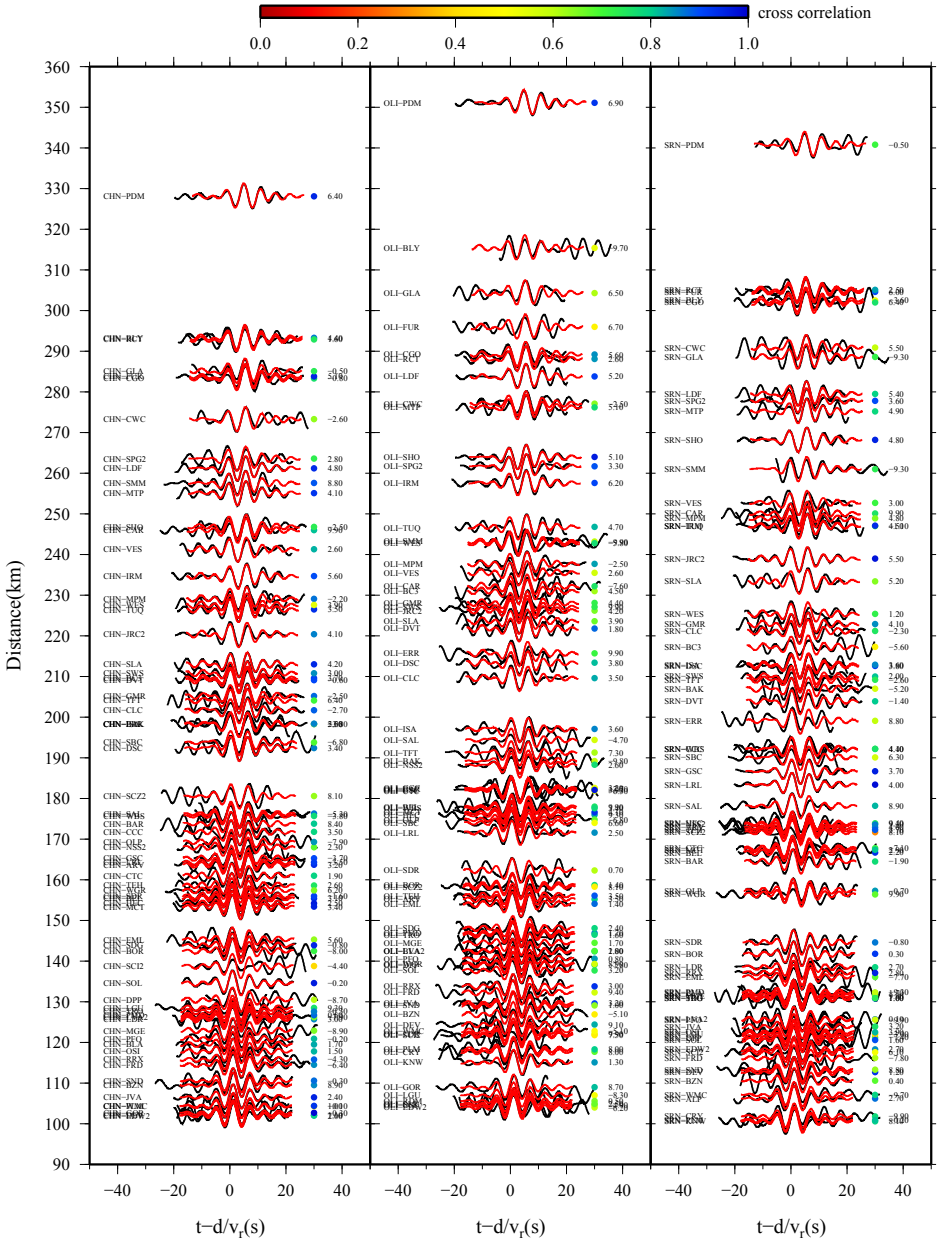

Figure 2.10: The same as Figure 2.8, but for 5-10s Z-Z NCFs (Rayleigh waves). A reduction velocity of Vr=3.1km/s is used since the shallower crust is involved.

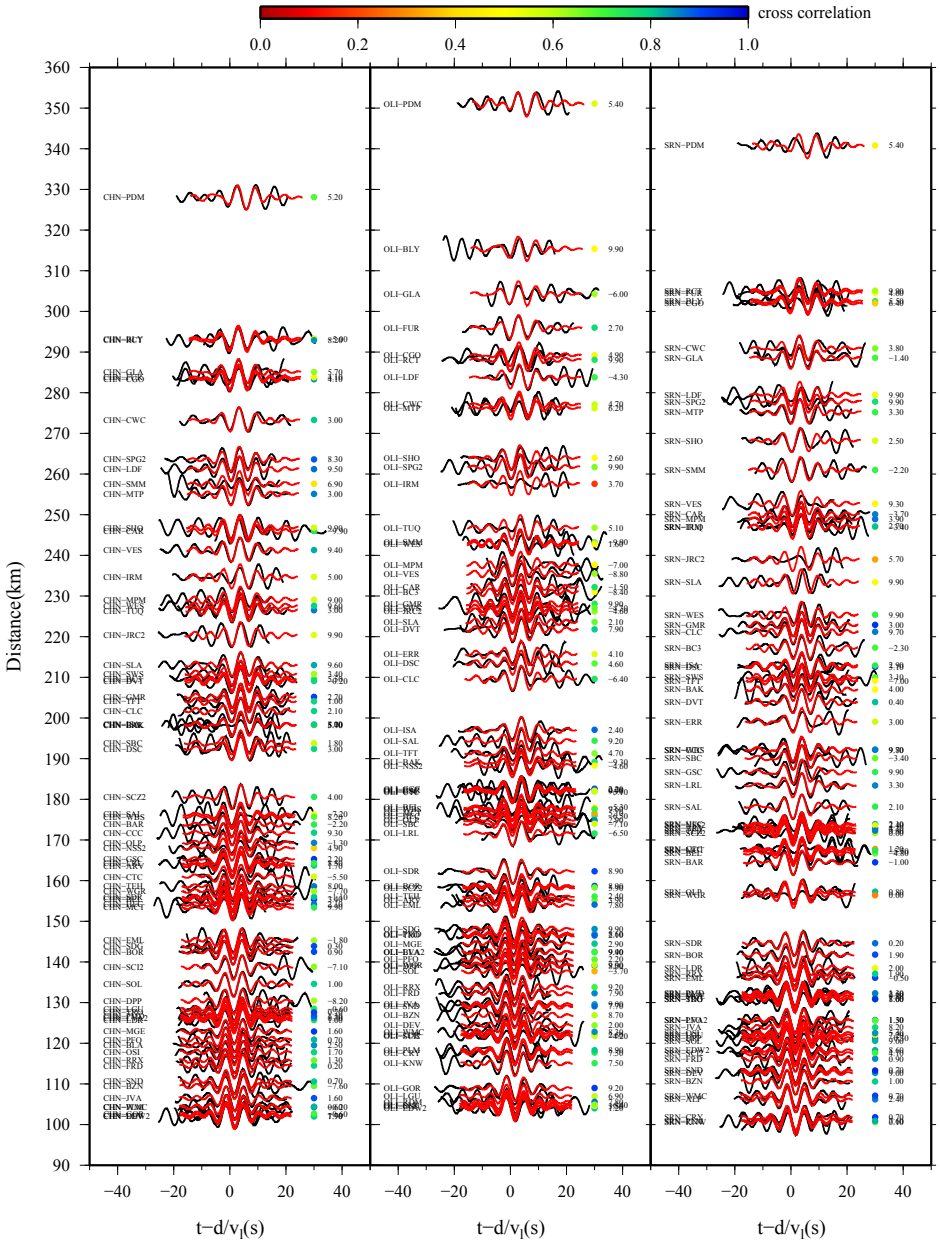

Figure 2.11: The same as Figure 2.8, but for 5-10s T-T NCFs (Love waves). A reduction velocity of Vl=3.4km/s was used in the case.

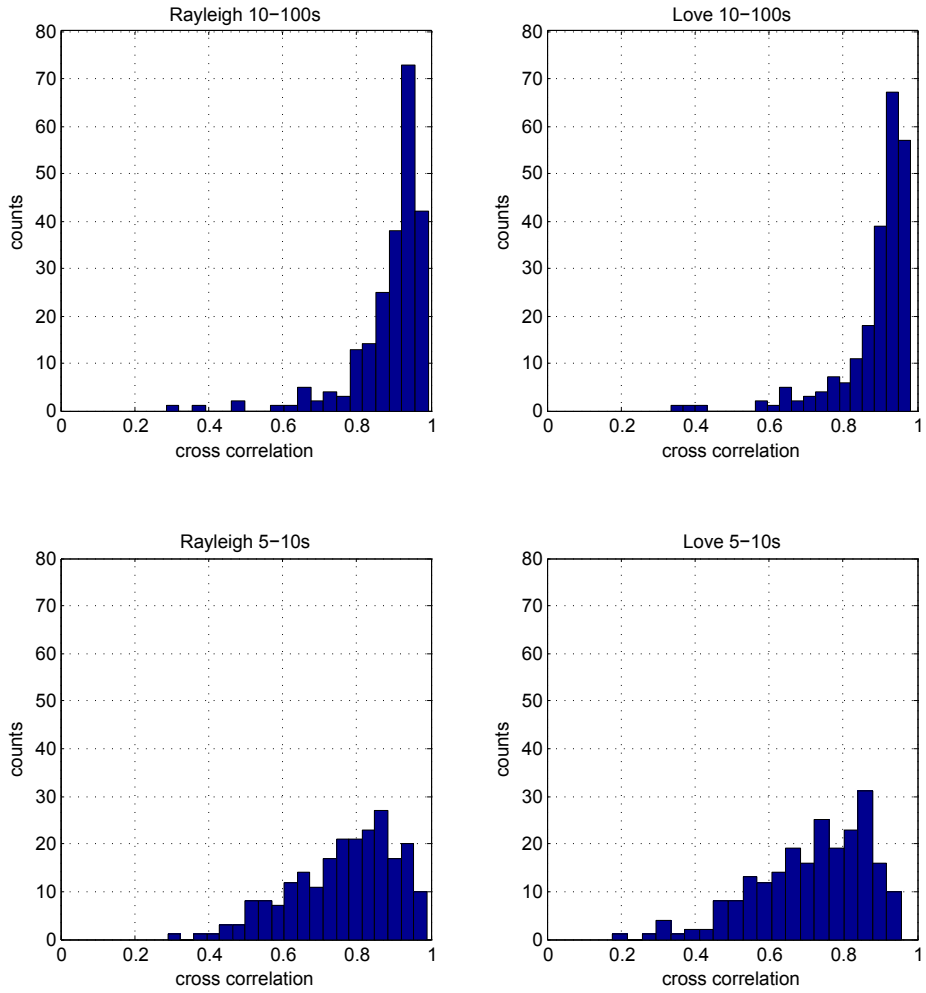

Figure 2.12: Histograms of the cross correlation coefficients between NCFs and 1D synthetic seismograms, for 5-10s, 10-100s Rayleigh and Love waves. The percentages of NCFs with cross correlation coefficients larger than 0.8 are 88% for 10-100s Rayleigh and Love waves, but 47% and 36% for 5-10s Rayleigh and Love waves, respectively.

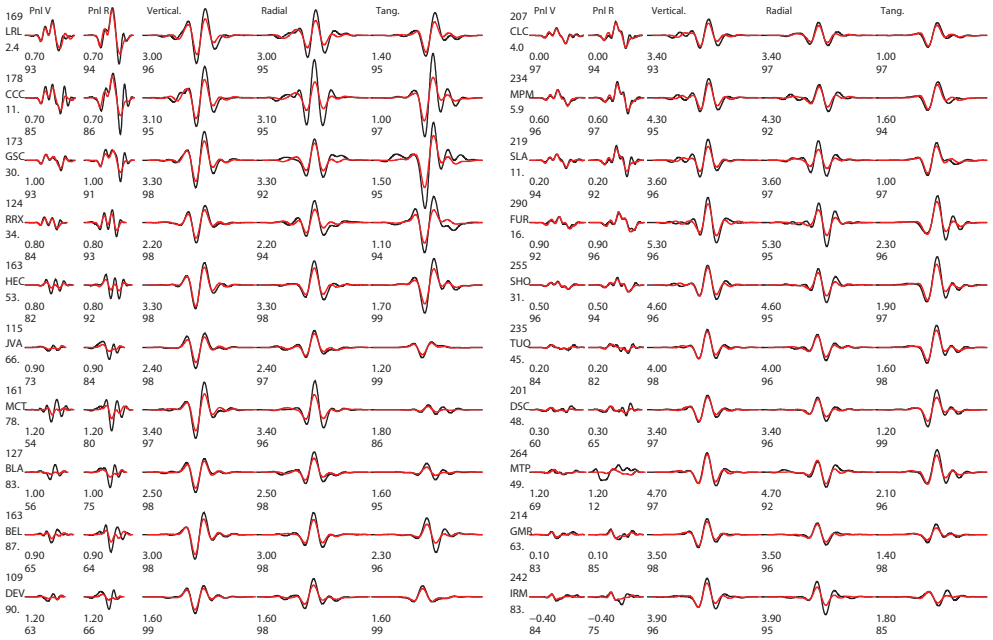

Figure 2.13: Example comparison of synthetic (red) and data (black) for the Chino Hills event at stations in the northeastern direction. The name of station is at the left of each seismogram, the number above the station name is epicenter distance in kilometer and below is azimuth. The number on the lower left of the seismograms are the time shifts (upper) and cross-correlation coefficients in percent (lower). Positive time shifts indicate slow paths. Pnl waves are filtered with bandpass (0.02~0.2 Hz) and surface waves are filtered with (0.01~0.1 Hz), a Standard South California Model (SoCal) is used.

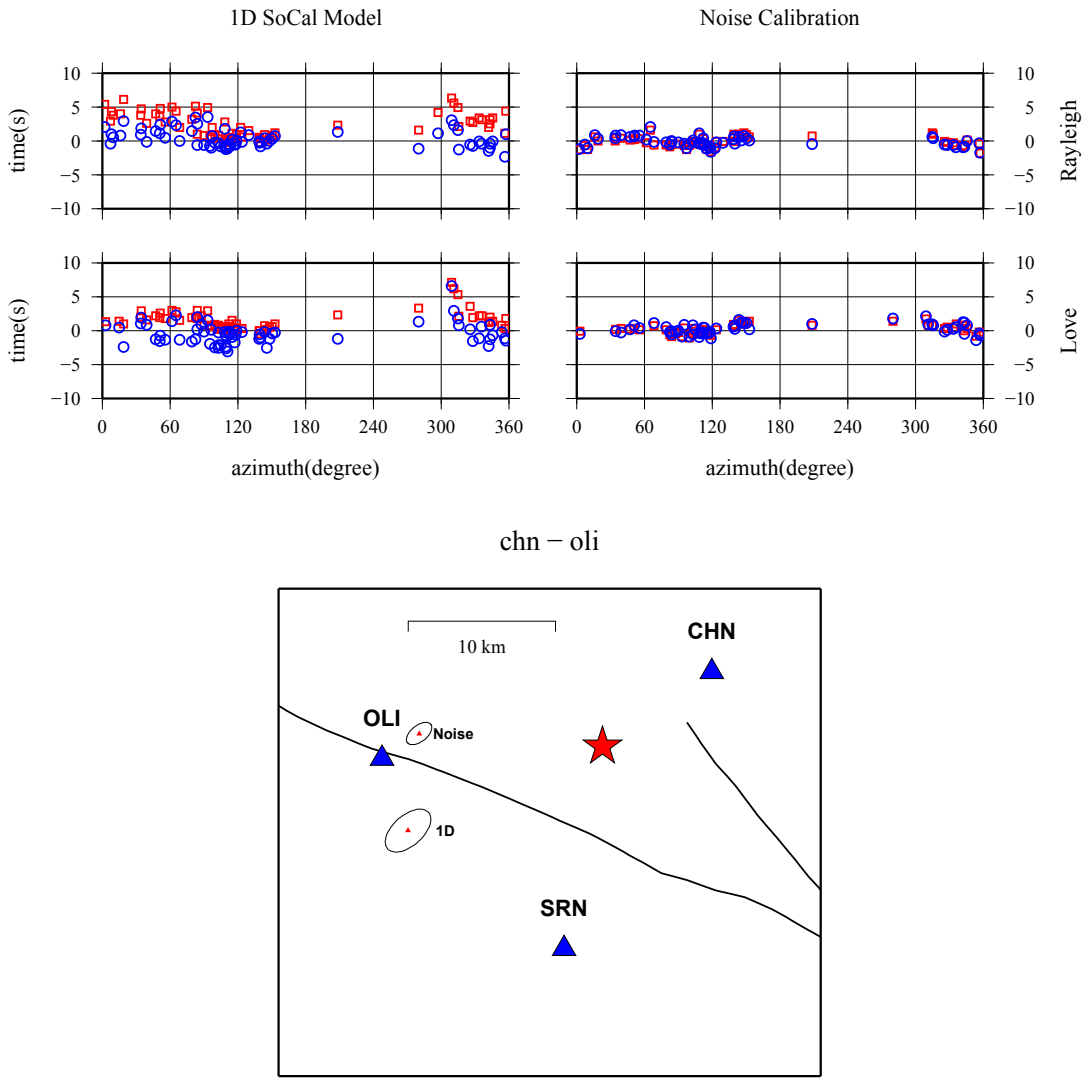

Figure 2.14: Locate virtual source OLI with 1D SoCal model (upper left column) and noise calibration from virtual source CHN (upper right column). Red squares and blue circles are time shifts before and after the relocation respectively. Results are shown in map view as red triangles with 95% confidence limits (black ellipses). Black lines are the Whittier Fault and Chino Fault.

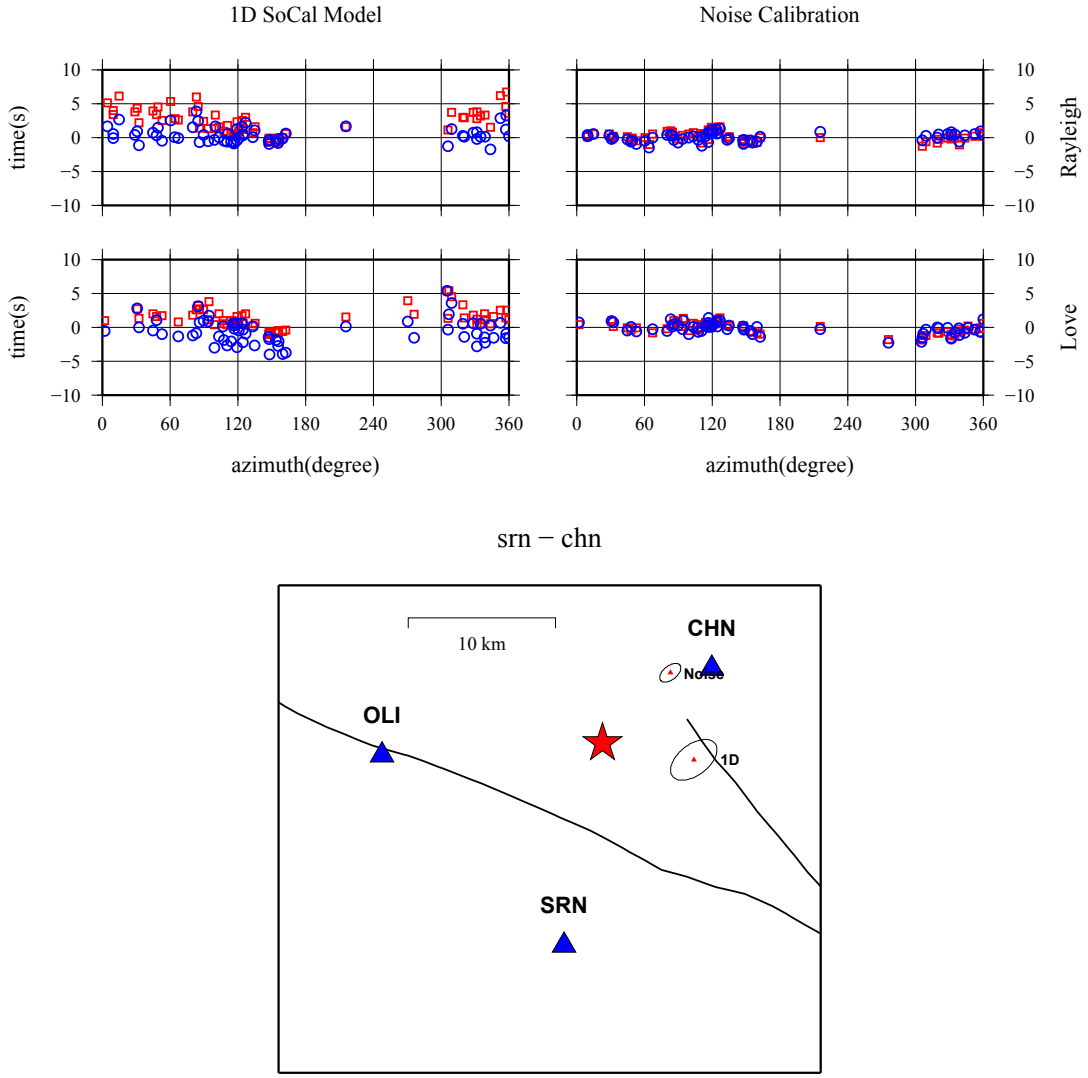

Figure 2.15: The same as Figure 2.14, but for locating CHN with 1D SoCal model and calibration from SRN.